Proceedings of the 21st ICSMGE, Vienna, Austria, 14 – 19 June 2026. Pistrol, Adam & Schweiger (eds.)
Published by: ÖGG, Austrian Society for Geomechanics, Salzburg, Austria, ISBN 978-3-9503898-4-5
https://doi.org/10.53243/ICSMGE2026-383

Enhancing surface wave site characterization by full-wavefield inversion

Chih-Ping Lin, Tsai-Jung Wu, Quoc Kinh Tran, Ernian Pan
Department of Civil Engineering, National Yang Ming Chiao Tung University, Hsinchu, Taiwan, cplin.ce@nycu.edu.tw

ABSTRACT: Site characterization is essential for geotechnical and earthquake engineering design and risk assessment. The multichannel analysis of surface waves (MASW) method efficiently provides subsurface layer structures and shear wave velocity (V_S) profiles but is inherently non-linear and mathematically ill-posed, allowing multiple models to fit the data equally well. Current MASW inversions primarily rely on modal dispersion curves, especially the fundamental mode (FM), rather than utilizing the complete wavefield information. This simplification often introduces significant epistemic uncertainty, reflected in the variability of inversion results due to choices in the number of layers (L_n) and maximum resolvable depth (z_{max}). To address these challenges, we propose a full-wavefield inversion approach that incorporates both amplitude and phase information from the entire wavefield. Phase data are used to derive the V_S profile, while amplitude data enable estimation of material damping. This method eliminates the need for dispersion curve picking, accounts for survey configurations, and captures all propagating modes, reducing uncertainty and mode misidentification. By systematically varying L_n and z_{max}, we quantify the spread of inversion results across different layer parameterizations to reveal the epistemic uncertainty inherent in the inversion process. Results show that full-wavefield inversion improves accuracy, reduces model bias, enhances depth resolution, and provides both Vs and damping ratio profiles for a more comprehensive subsurface characterization. This framework offers a robust tool for advancing MASW applications in geotechnical and earthquake engineering.

KEYWORDS: Shear wave velocity, MASW, full-wavefield inversion, uncertainty, damping ratio.

1 INTRODUCTION

Surface wave methods are widely used in geotechnical engineering due to their efficiency in characterizing near-surface conditions. These methods are commonly adopted to infer shear wave velocity (V_S) profiles, which are directly related to the shear modulus. Various surface wave methods have been developed for near-surface site characterization, and can be classified based on their data acquisition techniques and corresponding dispersion analysis. Among these, multichannel analysis of surface waves (MASW) is a widely adopted approach that captures the wavefield generated by an active source at multiple locations along the ground surface. The dispersion relation can be determined using various techniques. When the receiver array is sufficiently long, current practice assumes that the modal modes can be identified, and inversion is typically performed based on one or more modal modes, particularly the fundamental mode (FM). However, MASW-measured dispersion curves use only a portion of the wavefield information and may deviate from the true modal modes due to truncation effects. Additionally, some dominant modes may not correspond to any of the theoretical modal modes (Lin et al. 2023). To address the aforementioned issues, several studies have performed inversion by fitting the measured data in transformed domains, such as the frequency–slowness and frequency–velocity domains (Forbriger, 2003; Ryden & Park 2006; Zhang et al. 2024). This approach can be considered as a type of full-wavefield inversion. Lin et al. (2022) proposed a fast algorithm for computing dynamic response in the frequency domain, upon which a more rigorous inversion scheme was developed to invert the full frequency–velocity spectrum from multichannel data. This method was further refined and applied in subsequent work, where it was compared with two practical approaches: effective mode inversion in spectral analysis of surface waves (SASW) and MASW FM inversion (Lin et al. 2024).

Current surface wave methods primarily focus on inverting Vs profiles. Although recent studies have investigated the damping ratio (D) profiles (Aimar et al. 2024), also an important parameter for earthquake engineering analysis, accurately accounting for geometric spreading remains challenging without access to the full elastic wavefield. In this study, V_S profiles obtained from FM and FVS inversion under different layer parameterizations are presented and compared using synthetic examples to illustrate both epistemic uncertainty and the influence of damping ratio. Additionally, D profiles are inverted using a rigorous full-wavefield approach.

2 FULL-WAVEFIELD COMPUTATION, FVS, AND FAS

For a multi-layered half-space subjected to a unit vertical circular load applied on the ground surface (Figure 1), the vertical displacement field on the same surface is denoted as $w(t, r)$, representing its variation with respect to time (t) and radial distance (r). By applying Fourier transform with respect to t and Hankel transform (Fourier-Bessel transform) with respect to r, and leveraging the axial symmetric condition, the Green's function in the transformed domain, $\hat{w}(\omega, k)$, can be solved (Lin et al. 2022). The frequency response (i.e., the response to time-harmonic loading) is then obtained by applying the inverse Hankel transform to the Green's function:

$$W(f,r) = \int_0^\infty \hat{w}(f,k)\hat{S}(k)J_0(kr)kdk \tag{1}$$

where f is frequency, k is wavenumber, J_0 is the Bessel functions of the first kind of order 0, and $\hat{S}(k)$ is the Hankel transform of the spatial variation of the load.

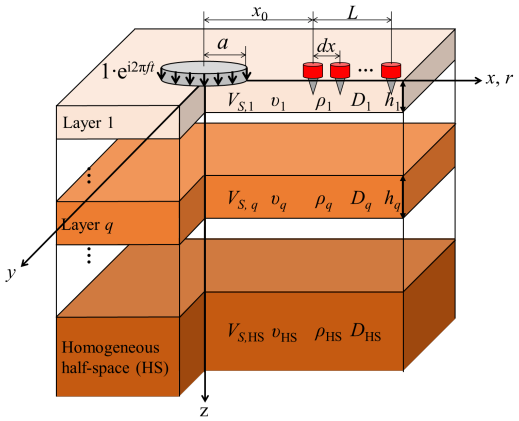

Figure 1. Schematic of the layered model subjected to circular loading.

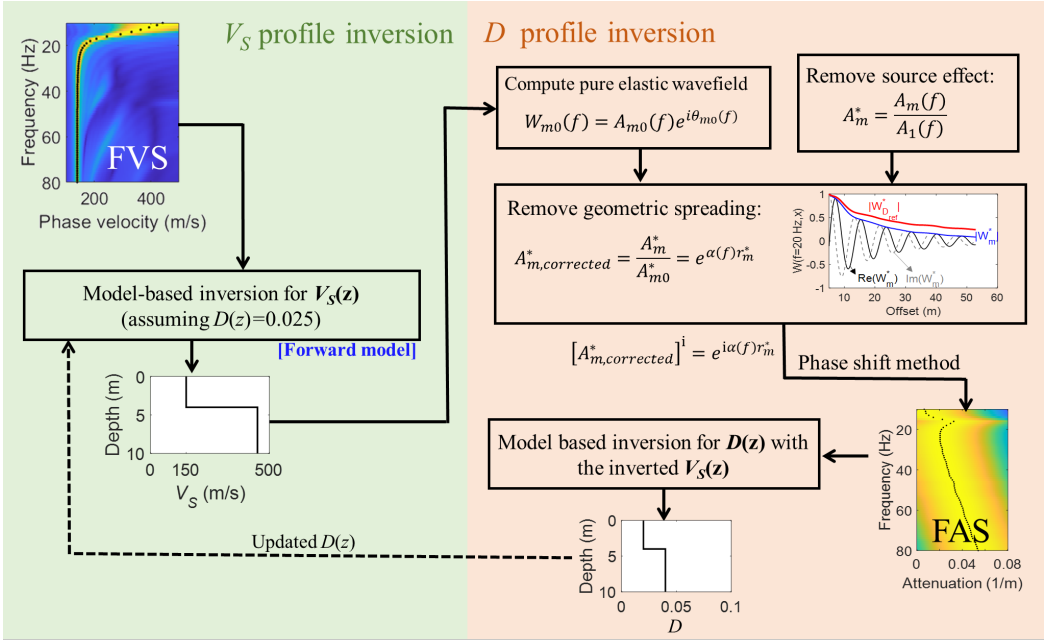

Figure 2. A flow chart showing how the full wavefield can be decomposed into FVS and FAS, and iteratively inverted for Vs and D profiles.

For efficient numerical computation, the Hankel transform can be approximated using a Fourier–Bessel series. This discretization replaces the continuous wavenumber in the wavefield with discrete values k_m, where k_m is determined by the m-th zero of the Bessel function scaled by the maximum radius R, where $J_0(k_mR)=0$, and truncated at a large number (M). As a result, the computationally expensive numerical integration required for the inverse Hankel transform can be replaced by a more efficient Fourier–Bessel series expansion:

$$W(f,r) = \sum_m \hat{w}(f,k_m)\hat{S}(k_m)J_0(k_m r) \quad (2)$$

This dynamic response of an isotropic elastic layered half-space subjected to a vertical loading was implemented and thoroughly validated by Lin et al. (2022). The proposed algorithm preserves the complete wavefield, including the near-field effect and leaky waves, and is at least two-orders of magnitude faster than the conventional integration-based transformation method. This significant improvement facilitates full-wavefield inversion in the transformed spectrum domain.

To compute the dispersion spectrum as a function of frequency and phase velocity, the phase-shift method proposed by Park et al. (1998) is used:

$$\hat{W}(f,v) = \sum_m W(f,r_m)\Big/\left|W(f,r_m)\right| \cdot e^{i\frac{2\pi f}{v}r_m} \quad (3)$$

where r_m is the source-to-receiver distance of the m^{th} receiver, and v is the phase velocity. The normalized amplitude component of $\hat{W}(f,v)$, obtained by normalizing with respect to the maximum amplitude at each frequency, is referred to as the frequency–velocity spectrum (FVS).

As illustrated schematically in Figure 2, the recorded wavefield can be decomposed into a phase shift ($\theta_m(f)$) and amplitude decaying with the source-to-receiver offset ($A_m(f)$), such that $W_m(f)=A_m(f)e^{i\theta m(f)}$. The FVS represents the phase shift information extracted from the wavefield and is primarily governed by the Vs profile. It is generally insensitive to Poisson's ratio (υ), density (ρ), and D. As shown in Section 3, V_S profiles can be inverted from FVS by assuming reasonable values for Poisson's ratio, density, and D.

In contrast to phase information, the amplitude of wavefield decreases with increasing source-to-receiver offset due to geometric spreading and material damping. To isolate material damping, the effects of the source and geometric spreading must first be corrected. The source effect is removed by normalizing the amplitude at each receiver location with respect to that of the first receiver. Geometric spreading is addressed by computing the corresponding pure elastic response based on the estimated V_S profile from FVS inversion. Finally, the observed amplitudes at receiver locations are divided by their respective elastic responses, thereby eliminating the effects of geometric spreading.

After eliminating the effect of source function and geometric spreading, the amplitude decay with the offset r follows $A(r)=e^{\alpha(f)r}$, where $\alpha(f)$ is the frequency-dependent attenuation coefficient. By raising $A(r)$ to the power of i (where $i=\sqrt{-1}$), i.e., $[A(r)]^i=e^{i\cdot\ln A(r)}$, the attenuation spectrum $\alpha(f)$ can be analyzed using the same wavefield transformation method as that used for FVS. This frequency-attenuation spectrum (FAS) can then be used to invert the D profile. The FVS inversion can be iteratively refined using the D profile obtained from prior inversion, followed by an updated FAS inversion. A few iterations can be performed to fit both the FVS and FAS, enabling a true full-wavefield inversion. Two synthetic Earth models (Table 1) are used to demonstrate the proposed inversion scheme, with the corresponding results presented in Section 3.

Table 1. Parameters of two synthetic Earth models

Model	Layer	h (m)	V_S (m/s)	D
1	1	4	150	0.04
	2	Inf	450	0.02
2	1	4	200	0.03
	2	4	150	0.05
	3	3	240	0.03
	4	Inf	320	0.02

Note: The density and Poisson's ratio are fixed at 2000 kg/m^3 and 1/3, respectively.

3 INVERSION OF SHEAR WAVE VELOCITY PROFILE

3.1 *Model parameterization and initial model*

Parameterization is the first step in the inversion process and it involves determining the maximum resolvable depth (z_{max}) and number of layers (L_n, including half-space). The inversion becomes highly nonlinear when both V_S and layer thickness (h) are treated as free parameters. To reduce complexity, a practical scheme is adopted in which the profile is divided into several layers, and only V_S is inverted. Several values of z_{max} and L_n are tested, with L_n ranging from 2 to 8 layers for each z_{max}. The thickness of each layer is determined by the ratio of z_{max}, as shown in Figure 3, and the corresponding V_S profile is then inverted. For a given z_{max}, the final inverted result is selected according to the principle of parsimony, favoring a simpler model with fewer parameters when multiple models fit the data equally well. The inverted results from different combinations of z_{max} and L_n are presented to show the uncertainty associated with model parameterization.

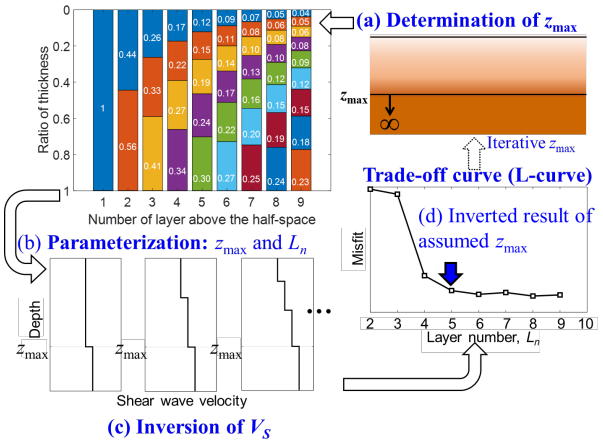

Figure 3 Illustration of parameterization and inversion process. For an assumed z_{max}, inversion results are obtained for different L_n values. The preferred results are selected based on the principle of parsimony.

The initial model for inversion is estimated by the simplified inversion method that directly converts the apparent dispersion curve to V_S profile (Pelekis & Athanasopoulos 2011; Lin et al. 2024). The apparent dispersion curve in the frequency–velocity spectrum is first transformed into wavelength (λ) and v domain. Then, it is further transformed into apparent depth (z_{app}) and apparent shear-wave velocity ($V_{S,app}$) by converting λ to the apparent depth, $z_{app}=0.5\lambda$, and taking the apparent shear-wave velocity as $V_{S,app}=v/0.9$.

3.2 *FM inversion and FVS inversion*

MASW fundamental mode (FM) inversion assumes that the measured dispersion curve from multi-station signals represents the fundamental mode. The objective function (Φ_{FM}) for the FM inversion is defined as:

$$\Phi_{FM} = \sum_f \left(v_m(f) - v_{FM}(f)\right)^2 \quad (4)$$

where $v_m(f)$ is the picked FM dispersion curve from the measured FVS peaks; $v_{FM}(f)$ is the theoretical FM. It should be noted that $v_{FM}(f)$ is independent of the source and receiver locations.

MASW FVS inversion infers the V_S profile by directly fitting the theoretically predicted FVS, computed using the dynamic response solution (i.e., Eq. (2)), to the measured FVS obtained from the Fourier transform of the shot records. The objective function (Φ_{FVS}) for the FVS inversion is defined as:

$$\Phi_{FVS} = 1 - \frac{\sum_{i=1}^{I}\sum_{j=1}^{J}\left|FVS_m(f_i,v_j)\right|\times\left|FVS_p(f_i,v_j)\right|}{\sqrt{\sum_{i=1}^{I}\sum_{j=1}^{J}\left|FVS_m(f_i,v_j)\right|^2}\sqrt{\sum_{i=1}^{I}\sum_{j=1}^{J}\left|FVS_p(f_i,v_j)\right|^2}} \quad (5)$$

where FVS_m and FVS_p represent the measured and predicted FVS, respectively. Indices i and j denote summation over frequency and phase velocity, respectively. A build-in local search algorithm (fminsearch.m) in MATLAB is used for finding the best fit in FM and FVS inversion.

3.3 *V_S inversion results assuming a constant damping ratio*

Wu et al. (2025) presented a comparison of the epistemic uncertainty arising from model parameterization in FM and FVS inversions; however, the influence of damping ratio was not addressed. In this study, in addition to model parameterization, the effect of damping ratio is also examined using synthetic Earth models. Since the actual damping ratio of each layer is unknown (see D in Table 1), an elastic assumption (i.e., D=0) is made for FM inversion, while a constant damping ratio (D=0.025) is assumed for FVS inversion. During both inversion processes, Poisson's ratio and density are assumed to be 1/3 and 2000 kg/m^3, respectively.

A simple two-layer model with a high V_S contrast (Model 1 in Table 1) is examined using these two different inversion approaches: FM and FVS inversions. The measured spectrum is shown in Figure 4a1, with the FM and the first higher mode of the actual profile depicted as solid lines. In this type of profile, dispersion energy may be dominated by the first higher mode below a certain frequency. This dominance can extend into lower frequencies as a leaky mode (fast-guided waves), where no roots exist in the dispersion equation (Lin et al., 2023). For FM inversion, spectral peaks (the black dots in Figure 4a1) are extracted and used, whereas for FVS inversion, the entire spectrum amplitude is utilized. Inverted V_S profiles using the preferred L_n with different assumed z_{max} values are presented in Figure 4b1 and 4c1 for FM and FVS inversions, respectively. Compared to the inverted results in Wu et al. (2025), the damping ratio appears to have only limited influence on V_S inversion when a reasonable value is assumed (even it does not match the true value). The effect of an incorrect damping ratio can be observed in the dispersion image, particularly in the regions indicated by the red arrows in Figure 4a1 and d1. However, this discrepancy has minimal impact on the overall FVS inversion results. Comparing Figure 4c1 and 4b1, FVS inversion yields more accurate and consistent results, as it accounts for the actual dynamic response at receiver locations. In contrast, FM inversion significantly overestimates V_S in the lower half-space, primarily due to the misidentification of the FM.

A multi-layered profile with an embedded soft layer (Model 2 in Table 1) is also examined. This type model is not uncommon in site conditions where higher stiffness is observed above the groundwater table. In this scenario, the dominant mode transitions to higher modes as frequency increases (Figure 4a2). FM inversion discards the higher-mode information at higher frequencies (i.e., smaller wavelengths). As a result, it produces reasonable inverted profiles but with reduced spatial resolution at shallow depths (Figure 4b2). On the other hand, the best FVS inverted profile (the thickest line in Figure 4c2) closely matches the actual profile, despite the use of a constant damping ratio that differ from the actual D profile. The FVS inversion results in Figure 4c2 exhibit lower model uncertainty than those in Figure 4b2, due to the use of full dispersion spectrum amplitude rather than relying solely on spectral peaks.

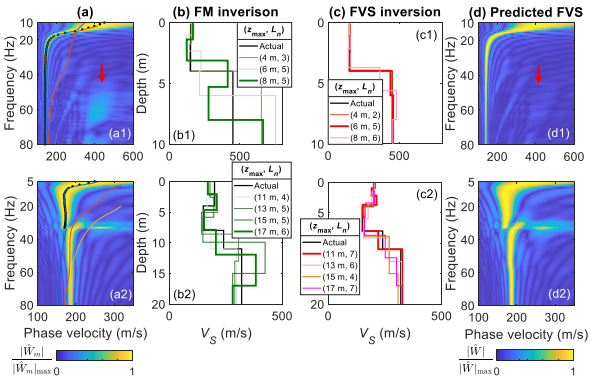

Figure 4 (a) The measured spectrum, with black dots indicating the spectral peaks used for FM inversion. Solid lines represent the modal dispersion curves. (b) FM inversion results. (c) FVS inversion results. The thickest profiles in (b) and (c) correspond to the profiles with the smallest misfit values among the preferred profiles. (d) The predicted FVS of the thickest inverted V_S profile shown in (c), assuming a constant damping ratio D=0.025.

4 INVERSION OF DAMPING RATIO PROFILE

In the previous section, only the phase information of the wavefield was used to infer the V_S profile. In this section, FAS inversion is applied to estimate the D profile following FVS inversion (see Figure 2). The layer parameterization used for FAS inversion is identical to that of the best inverted V_S profiles from FVS inversion (i.e., the thickest profiles in Figure 4c), which are also used to compute the elastic wavefield. After removing the source function and geometric spreading effects, the experimental FAS can be calculated. The misfit function remains the same as in Eq. (5) but is formulated in the frequency-attenuation domain. The initial damping ratio models (dashed lines in Figure 5a) are generated by mapping the damping ratio range [0.01 0.05] to the inverted V_S profile, with 0.01 assigned to the maximum V_S and 0.05 to the minimum V_S, followed by interpolation. This approach is based on the commonly observed relationship that a softer material, characterized by lower V_S, generally exhibits a higher damping ratio.

Figure 5 presents the inverted D profiles for Models 1 and 2 after two iterations of FVS and FAS inversions (see Figure 2), along with their corresponding FAS. For Model 1, the inverted D profile closely matches the actual D profile after the second iteration. In contrast, the inverted D profile for Model 2 captures the overall trend of the actual D profile but exhibits some deviation. The sensitivity of FAS to complex D profiles should be further investigated.

5 CONCLUSIONS

Two inversion approaches, FM and FVS inversions, are applied to examine the epistemic uncertainty arising from layer parameterization in the absence of knowledge of the actual damping ratio (D). The inversion results indicate that D has a limited influence on the estimation of shear-wave velocity (V_S). Then, an FAS inversion process is proposed to estimate the D profile. Iterative FVS-FAS inversion can be performed to refine the estimation of V_S and D.

FVS inversion, which accounts for the full dynamic response at receiver locations, incorporates possible higher modes and non-Rayleigh wave contributions. As a result, the inverted V_S results obtained under different layer parameterizations exhibit lower model uncertainty and provide more accurate estimations when compared to FM inversion, as demonstrated in the synthetic examples.

The inverted D profile from the two synthetic models demonstrated the effectiveness of the proposed iterative FVS-FAS inversion scheme for joint estimation of the V_S and D profiles. Further validation using additional synthetic and field examples is necessary to evaluate the accuracy and reliability of the method. Alternative model parameterizations and inversion algorithms will also be explored in the future work.

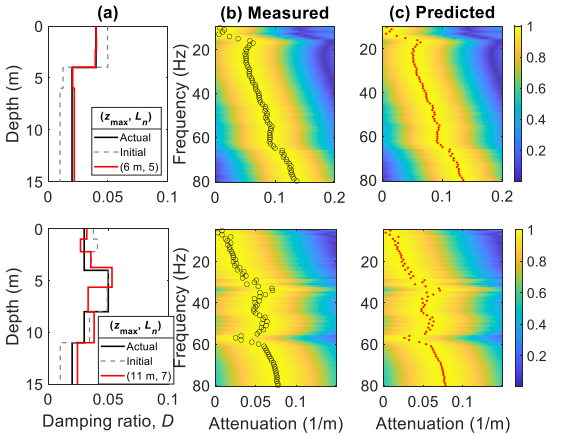

Figure 5 (a) The actual and inverted D profiles. (b) The measured FAS and (c) the predicted FAS, both after removing the source function and geometric spreading effects.

6 REFERENCES

Aimar, M., Foti, S., and Cox, B. R. 2024. Novel techniques for in situ estimation of shear-wave velocity and damping ratio through MASW testing part II: a Monte Carlo algorithm for the joint inversion of phase velocity and phase attenuation. *Geophysical Journal International* 237, 525–539.

Forbriger, T. 2003. Inversion of shallow-seismic wavefields: II. Inferring subsurface properties from wavefield transforms. *Geophysical Journal International* 153, 735–752.

Lin, C. P., Pan, E., Tran, Q. K., and Wu, T. J. 2023. A unified approach for relationships among Green's function, normal modes and dispersion spectrum in layered elastic half-space, with corrected misconceptions on surface wave dispersion and testing. *Geophysical Journal International* 232, 1357–1375.

Lin, C. P., Wu, T. J., and Pan, E. 2022. An efficient full-wavefield computational approach for seismic testing in a layered half-space. *Soil Dynamic and Earthquake Engineering* 161, 107423.

Lin, C. P., Wu, T. J., Pan, E., and Tran, Q. K. 2024. Full-wavefield surface wave method: integrating rigorous and efficient methods for enhanced subsurface exploration. Journal of Geotechnical and Geoenvironmental Engineering 150, 04024021.

Park, C. B., Miller, R. D., and Xia, J. 1998. Imaging dispersion curves of surface waves on multi-channel record. SEG Technical Program Expanded Abstracts, 1377–1380.

Pelekis, P. C. and Athanasopoulos, G. A. 2011. An overview of surface wave methods and a reliability study of a simplified inversion technique. *Soil Dynamics and Earthquake Engineering* 31, 1654–1668.

Ryden, N., and Park, C. B. 2006. Fast simulated annealing inversion of surface waves on pavement using phase velocity spectra. *Geophysics* 71, R49–R58.

Wu, T. J., Lin, C. P., Pan, E., and Tran, Q. K. 2025. Quantifying uncertainty in MASW inversion and uncertainty reduction through dispersion-spectrum inversion. *Soil Dynamics and Earthquake Engineering* 197, 109523.

Zhang, Z., Alkhalifah, T., and Liu, Y. 2024. Full dispersion-spectrum inversion of surface waves. *Journal of Geophysical Research: Solid Earth* 129, e2023JB028469.